Journal of Power Sources 206 (2012) 47–52

Contents lists available at SciVerse ScienceDirect

Journal of Power Sources

journal homepage: www.elsevier.com/locate/jpowsour

Novel triple-phase composite cathode materials for proton-conducting solid oxide fuel cells

Qiumei Jiang [a], Jigui Cheng [a,*], Rui Wang [a], Yumeng Fan [a], Jianfeng Gao [b]

[a] School of Materials Science and Engineering, Hefei University of Technology, Hefei, Anhui 230009, PR China
[b] Department of Materials Science and Engineering, University of Science and Technology of China, Hefei, Anhui 230026, PR China

ARTICLE INFO

Article history:
Received 3 November 2011
Received in revised form 8 January 2012
Accepted 12 January 2012
Available online 21 January 2012

Keywords:
Proton-conducting solid oxide fuel cells
Composite cathode
Proton conductor
Sinterability
Electrochemical performance

ABSTRACT

$Ce_{0.8}Sm_{0.2}O_{2-\delta}$ (SDC), $BaZr_{0.1}Ce_{0.7}Y_{0.2}O_{3-\delta}$ (BZCY) powders are mechanically mixed with $Sm_{0.5}Sr_{0.5}CoO_{3-\delta}$ (SSC) powders to prepare triple-phase SSC–*x*SDC–(0.3 – *x*) BZCY (*x* = 0.1, 0.15, 0.2) composite cathode materials for proton-conducting solid oxide fuel cells (H-SOFCs). The SSC, SDC and BZCY powders are all synthesized via aqueous gelcasting method. Chemical compatibility, sinterability, microstructure, linear thermal expansion coefficients, electrical conductivity and electrochemical performance of the composite cathode materials are investigated and compared with single phase SSC and dual-phase SSC–0.3BZCY composite cathode materials. The results reveal that there have no observable chemical reactions among SSC, SDC and BZCY after co-firing the powder mixes at 1100 °C for 3 h. Adding SDC and BZCY into SSC material decreases open porosity, increases the shrinkage rate of the sintered SSC materials and significantly reduces thermal expansion mismatch between BZCY and SSC materials. Electrical conductivity of the triple-phase composite cathode samples ranges from about 130.8 S cm^{-1} to 342.3 S cm^{-1} at temperature 450–800 °C, and increases as SDC content increases. Polarization resistances between the triple-phase composite cathode materials and the BZCY electrolyte decrease with increasing SDC content. The polarization resistance is significantly reduced from 1.57 Ω cm^2 for dual-phase SSC–0.3BZCY materials to 0.77 Ω cm^2 for triple-phase SSC–0.2SDC–0.1BZCY materials under open circuit conductions at 700 °C in air. The preliminary test results have suggested that triple-phase SSC–*x*SDC–(0.3 – *x*) BZCY (*x* = 0.1, 0.15, 0.2) materials may be a potential candidate of cathode material for H-SOFCs.

1. Introduction

Recently, much attention has been paid to the developments of proton-conducting solid oxide fuel cells (H-SOFCs) [1–4]. Compared with the oxide ionic conductors, the proton conductors have several advantages including the lower operating temperature impacting the life time of the cell components, the lower cost of the components required for the operation of the cell and the formation of water on the cathode side, which avoids fuel dilution and recycling and reduces risk of destructive anode oxidation even at high current densities [5]. In order to realize the practical applications of H-SOFCs, it is critical to achieve high powder density at reduced temperature. Besides, the development of new electrolyte materials with high proton conductivity, the reduction of electrolyte thickness and the development of cathode materials with low over-potential are also of great importance [6]. It has been demonstrated that the polarization resistance of the cathode materials becomes the major source of the cell resistance when the thickness of electrolyte is small enough. Therefore, the key work to improve the cell performance is to reduce the polarization resistance of the cathode materials [7].

Up to now, $BaZr_{0.1}Ce_{0.7}Y_{0.2}O_{3-\delta}$ (BZCY)-based H-SOFCs with different cathode materials have attracted much attention because BZCY is a good proton conductor, and efficient cathode materials have to be developed to make better use of the new proton conductors such as BZCY [8]. Many useful cathode materials, which operate at lower temperature, are based on cobalt-containing compounds, such as $Ba_{0.5}Sr_{0.5}Co_{0.8}Fe_{0.2}O_{3-\delta}$, $Sm_{0.5}Sr_{0.5}CoO_{3-\delta}$ (SSC) and $La_{0.6}Sr_{0.4}Co_{0.2}Fe_{0.8}O_{3-\delta}$ [6,7,9,10]. However, these cobalt-based oxides exhibit low structural stability and high thermal expansion coefficient, which restricts their further applications [11]. One way to solve this problem is to explore novel cobalt-free cathode materials. Another is to add a sufficient amount of electrolyte to the cobalt-based oxides to prepare composite cathode materials [9,11]. SSC–BZCY composite cathode material for H-SOFCs with BZCY electrolyte has been reported by Yang et al. [8]. However, the BZCY electrolyte material in the composite cathode possesses poor chemical stability standing against H_2O and CO_2. Water forms in the cathode for H-SOFCs and the cathode is also exposed to air. Although BZCY electrolyte material added in the SSC

* Corresponding author. Tel.: +86 551 2901793; fax: +86 551 2901793.
E-mail address: jgcheng63@sina.com (J. Cheng).

0378-7753/$ – see front matter © 2012 Elsevier B.V. All rights reserved.
doi:10.1016/j.jpowsour.2012.01.084

cathode material could improve the thermal compatibility between the BZCY electrolyte and SSC cathode, it weakens the long-term stability of the composite cathode. In order to solve this problem, it has been proposed that adding $Ce_{0.8}Sm_{0.2}O_{2-d}$ (SDC) instead of BZCY to the SSC cathode material to prepare SSC–SDC composite cathode for H-SOFCs with BZCY electrolyte can improve the thermal compatibility between BZCY electrolyte and the cathode materials and can improve the long-term stability of the cathode materials [9].

In this work, SDC and BZCY were added together into SSC to obtain triple-phase SSC–SDC–BZCY composite cathode materials to further improve the long-term stability and the thermal compatibility of BZCY electrolyte with the SSC cathode materials for H-SOFCs based on BZCY electrolyte. Chemical compatibility among SSC, SDC and BZCY was evaluated. And linear thermal expansion coefficients (TECs), electrical conductivity and microstructure of the triple-phase SSC–SDC–BZCY composite cathode materials were also measured and compared with those of the single phase SSC and the dual-phase SSC–BZCY composite materials. In addition, the interface resistances between the triple-phase SSC–SDC–BZCY composite cathode and BZCY electrolyte were investigated.

2. Experimental

2.1. Powder synthesis

$Sm_{0.5}Sr_{0.5}CoO_{3-\delta}$ (SSC), $Ce_{0.8}Sm_{0.2}O_{2-\delta}$ (SDC) and $BaZr_{0.1}Ce_{0.7}Y_{0.2}O_{3-\delta}$ (BZCY) powders were synthesized via an aqueous gelcasting method. Sm_2O_3, $SrCO_3$ and $Co(NO_3)_2{\cdot}6H_2O$ were used as raw materials for synthesizing SSC powder. The raw materials for the synthesis of SDC powder were Sm_2O_3 and $Ce(NO_3)_3{\cdot}6H_2O$. BZCY powder was prepared using $Ba(NO_3)_2$, $Zr(NO_3)_4{\cdot}5H_2O$, $Ce(NO_3)_3{\cdot}6H_2O$ and Y_2O_3 as the starting materials. For the preparation of each powder, stoichiometric amount of the raw materials were mixed in water with organic monomer (mixture of acryl amide (AM) and N, N′-methyl amide (MBAM), AM:MBAM = 20:1) by ball milling for 24 h to form dispersed suspensions. Ammonium bisulphate ($(NH4)_2S_2O_8$, APS) was then added into the suspensions and wet gels were obtained when heating the suspensions to about 80 °C. The wet gels were further heated to about 120 °C to remove the solvent water. SSC, SDC and BZCY powders were finally obtained after calcining the dried gels at 1100 °C for 3 h, 700 °C for 2 h and 1000 °C for 3 h, respectively.

SSC–*x*SDC–(0.3 − *x*) BZCY (*x* = 0, 0.1, 0.15, 0.2 of weight fraction) composite powders were prepared by a mechanical mixing process, in which the SSC, SDC and BZCY powders were ball milled in ethanol for 24 h. The dispersed suspensions were then dried at 60 °C to remove ethanol. After being ground, SSC–*x*SDC–(0.3 − *x*) BZCY (*x* = 0, 0.1, 0.15, 0.2) composite powders were finally obtained.

2.2. Samples preparation

Pure SSC cathode powders and SSC–*x*SDC–(0.3 − *x*) BZCY (*x* = 0, 0.1, 0.15, 0.2) composite powders were pressed uniaxially in a steel die under a pressure of 200 MPa to obtain slats (~50 mm in length, ~3 mm in width and ~3 mm in thickness). The green compacts were subsequently sintered at 1100 °C for 3 h for measurement of electrical conductivity, linear thermal expansion coefficient (TEC) and microstructure observation.

Symmetric cells for electrolyte–cathode interfacial resistance measurement with SSC and SSC–*x*SDC–(0.3 − *x*) BZCY (*x* = 0, 0.1, 0.15, 0.2) cathodes were prepared using a screen-printing technique with BZCY as the electrolyte. The procedures were summarized as follows: BZCY electrolyte powders were first pressed at 200 MPa into disks about 18 mm in diameter, and then sintered at 1450 °C for 5 h as electrolyte substrates. SSC and SSC–*x*SDC–(0.3 − *x*) BZCY (*x* = 0, 0.1, 0.15, 0.2) cathode slurries were prepared by ball-milling the SSC and SSC–*x*SDC–(0.3 − *x*) BZCY (*x* = 0, 0.1, 0.15, 0.2) cathode powders with a binder containing 6 wt.% ethyl cellulose-terpineol, respectively. These slurries were screen-printed onto each side of the sintered BZCY electrolyte substrates and then co-fired at 1100 °C for 3 h in air to form symmetric cathode/electrolyte/cathode cells.

2.3. Samples characterization

Phase composition of the triple-phase SSC–0.1SDC–0.2BZCY samples sintered at 1100 °C for 3 h in air was carried out by X-ray diffraction (XRD) analysis. Microstructure of the SSC and SSC–*x*SDC–(0.3 − *x*) BZCY (*x* = 0, 0.1, 0.15, 0.2) cathode samples sintered at 1100 °C for 3 h was observed by scanning electron microscope (SEM, Sirion 200). Linear thermal expansion coefficients (TECs) of the SSC and SSC–*x*SDC–(0.3 − *x*) BZCY (*x* = 0, 0.1, 0.15, 0.2) cathode specimens were measured from 50 °C to 800 °C using a dilatometer at a heating rate of 5 °C min^{-1} in air. Electrical conductivity of the sintered SSC and SSC–*x*SDC–(0.3 − *x*) BZCY (*x* = 0, 0.1, 0.15, 0.2) samples was tested by the four-probe method from 450 to 800 °C. AC impedance spectroscopy measurements of the symmetric cells with different cathode materials were carried out to investigate the polarization resistances via an electrochemical workstation (CHI604A). Ag paste was painted onto both sides of the symmetric cells and Ag wire was used as current collector. The frequency range varied from 1 Hz to 100 kHz with an AC signal amplitude of 10 mV. Measurement of the data was conducted in the temperature range of 500–700 °C at an interval of 50 °C. The electrochemical impedance spectra curves were simulated by the Zsimpwin software.

3. Results and discussion

3.1. Chemical stability

To evaluate the chemical stability of the triple-phase SSC–*x*SDC–(0.3 − *x*) BZCY (*x* = 0.1, 0.15, 0.2) composite cathode materials, SSC–0.1SDC–0.2BZCY samples sintered at 1100 °C for 3 h were ground into powders for XRD analysis. For comparison, phase structure of the SSC, SDC, BZCY powders was also carried

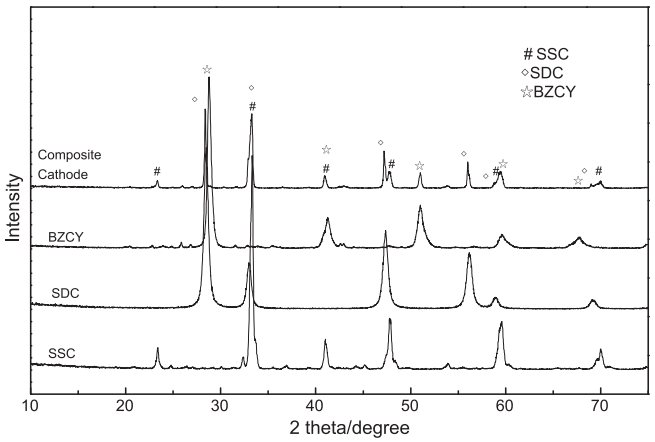

Fig. 1. XRD patterns of the SSC, SDC, BZCY powders and the SSC–0.1SDC–0.2BZCY samples calcined at 1100 °C for 3 h, 700 °C for 2 h, 1000 °C for 3 h and sintered at 1100 °C for 3 h, respectively.

Table 1
Sintering shrinkage and open porosity of the SSC and SSC–*x*SDC–(0.3 – *x*) BZCY cathode specimens sintered at 1100 °C for 3 h.

Cathode materials	Cathode composition			Sintering shrinkage (%)	Open porosity (%)
	SSC (wt.%)	SDC (wt.%)	BZCY (wt.%)		
SSC	100	0	0	3.35	33.89
$x = 0$	70	0	30	4.47	32.67
$x = 0.1$	70	10	20	4.8	30.24
$x = 0.15$	70	15	15	6.45	29.58
$x = 0.2$	70	20	10	6.92	18.48

out by XRD analysis. Fig. 1 shows XRD patterns of the SSC, SDC, BZCY powders and the SSC–0.1SDC–0.2BZCY sample calcined at 1100 °C for 3 h, 700 °C for 2 h, 1000 °C for 3 h and sintered at 1100 °C for 3 h, respectively. Only peaks corresponding to SSC (cubic perovskite), SDC (cubic fluorite) and BZCY (orthorhombic perovskite) are observed in the XRD patterns of the triple-phase SSC–0.1SDC–0.2BZCY composite cathode sintered at 1100 °C for 3 h. This suggests that there are no observable chemical reactions among SSC, SDC and BZCY after co-firing them at 1100 °C for 3 h, and it can be deduced that the triple-phase SSC–*x*SDC–(0.3 – *x*) BZCY ($x = 0.1$, 0.15, 0.2) composite cathode materials possess good chemical stability at 1100 °C.

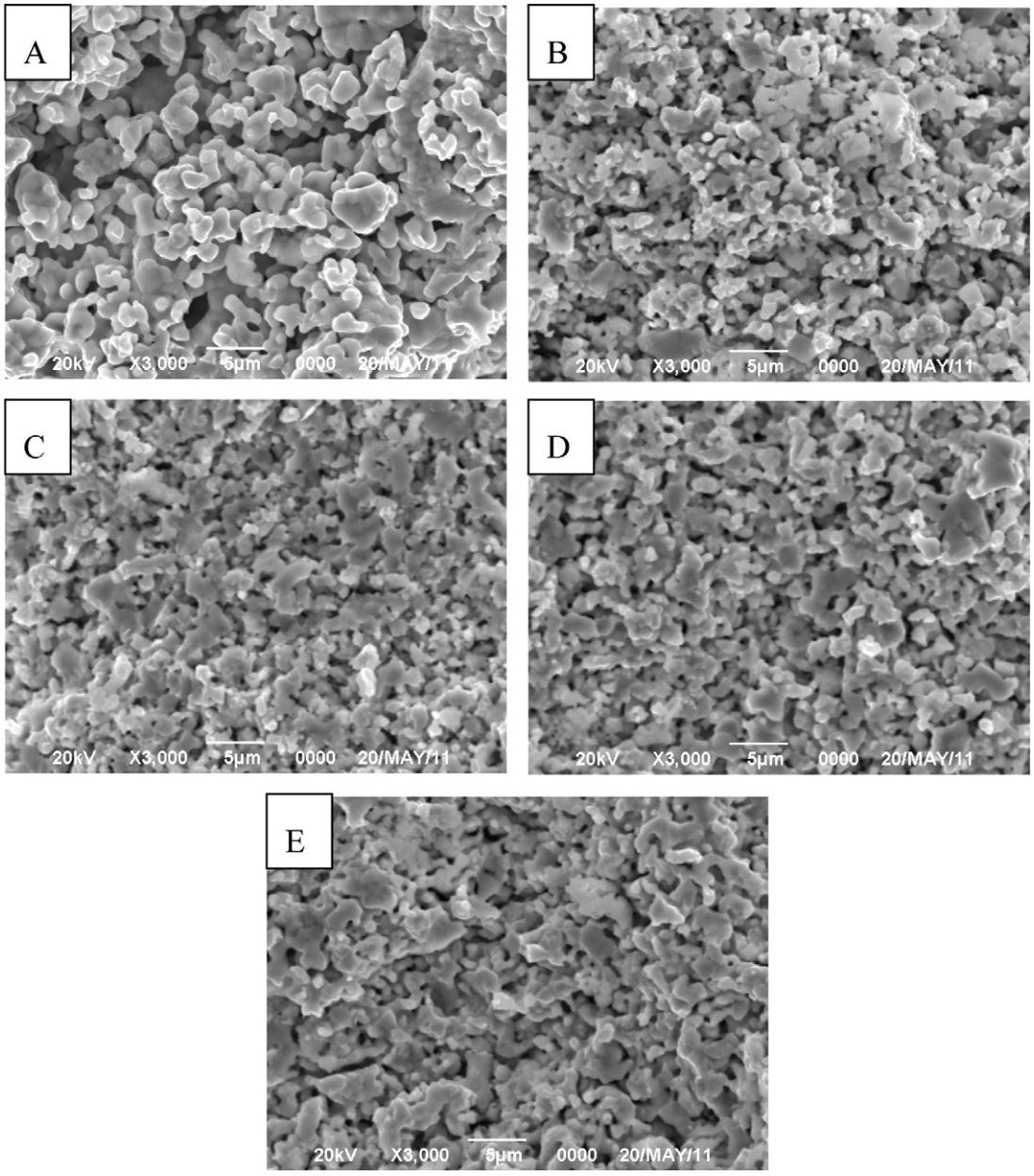

Fig. 2. SEM microstructure of the SSC and different SSC–*x*SDC–(0.3 – *x*) BZCY cathode specimens sintered at 1100 °C for 3 h: (A) SSC; (B) $x = 0$; (C) $x = 0.1$; (D) $x = 0.15$; (E) $x = 0.2$.

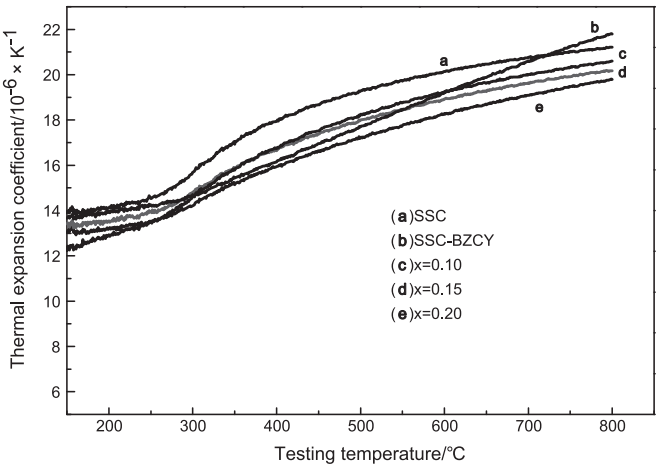

Fig. 3. Thermal expansion coefficients of the SSC and SSC–*x*SDC–(0.3 – *x*) BZCY cathode specimens sintered at 1100 °C for 3 h.

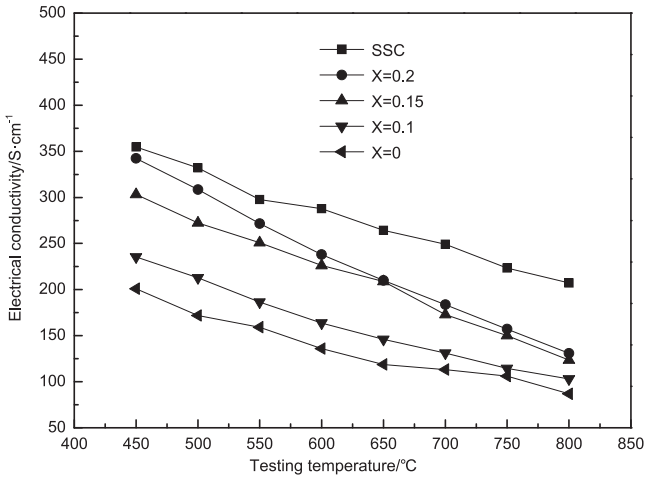

Fig. 4. Temperature dependence of electrical conductivity for the SSC and SSC–*x*SDC–(0.3 – *x*) BZCY cathode specimens sintered at 1100 °C for 3 h.

3.2. Sinterability and microstructure of the SSC–SDC–BZCY composite cathodes

Table 1 lists sintering shrinkage and open porosity of the SSC and SSC–*x*SDC–(0.3 – *x*) BZCY (*x* = 0, 0.1, 0.15, 0.2) cathode specimens sintered at 1100 °C for 3 h. As shown in Table 1, single phase SSC cathode samples without any addition of electrolyte exhibit the highest open porosity (33.89%) among all the samples. The dual-phase SSC–0.3BZCY composite cathode samples only added with BZCY electrolyte show less open porosity (32.67%) than that of the SSC samples, and the triple-phase SSC–*x*SDC–(0.3 – *x*) BZCY (*x* = 0.1, 0.15, 0.2) cathode specimens added with both SDC and BZCY electrolyte possess lower open porosity (30.24%, 29.58%, 18.48% for *x* = 0.1, 0.15, 0.2, respectively) than that of the SSC–0.3BZCY sample. Furthermore, open porosity of the triple-phase SSC–*x*SDC–(0.3 – *x*) BZCY (*x* = 0.1, 0.15, 0.2) cathode specimens decreases with the increase of SDC content. But the sintering shrinkage increases with the increase of SDC content. This reveals that addition of electrolyte ingredients into the SSC materials decreases the open porosity and increases the sintering shrinkage of the materials, and the addition of SDC has a more obvious effect.

Fig. 2 illustrates SEM images of the SSC and SSC–*x*SDC–(0.3 – *x*) BZCY (*x* = 0, 0.1, 0.15, 0.2) cathode specimens sintered at 1100 °C for 3 h. All the samples have porous microstructure. However, it is clearly seen that grain size of the SSC samples (Fig. 2(A)) is bigger than that of the composite cathode samples, which indicates that the addition of SDC and BZCY can restrain the grain growth of SSC during sintering. It is also shown in Fig. 2(B)–(E) that as SDC content increases in the SSC–*x*SDC–(0.3 – *x*) BZCY (*x* = 0, 0.1, 0.15, 0.2) composite materials, the specimens become denser and the grain size increases. This is consistent with the results listed in Table 1.

3.3. Thermal expansion coefficients

Thermal compatibility is a critical issue for cobalt-rich cathodes, which in general exhibit higher thermal expansion coefficient (TEC) values in the operation temperature range [12]. TEC curves of the SSC cathode samples sintered at 1100 °C for 3 h as function of testing temperatures is shown in Fig. 3. TEC values of SSC cathode changes slightly at first (<300 °C) and then increases rapidly as temperature increases (500–800 °C). Average TEC value of the SSC samples in temperature 200–800 °C is $21.7 \times 10^{-6}\,K^{-1}$, which is considerably larger than that of the BZCY electrolyte ($11.2 \times 10^{-6}\,K^{-1}$) [10]. This may result in the mismatch between the SSC cathode and the BZCY electrolyte during cell preparation and operation process. Fig. 3 also shows TEC curves of the SSC–*x*SDC–(0.3 – *x*) BZCY (*x* = 0, 0.1, 0.15, 0.2) composite cathode samples. TEC values for the triple-phase composite cathode materials increase slowly as temperature increases and the average TEC values (Table 2) in the temperature range of 200–800 °C is $18.3 \times 10^{-6}\,K^{-1}$, $18.0 \times 10^{-6}\,K^{-1}$ and $17.6 \times 10^{-6}\,K^{-1}$ for *x* = 0.1, *x* = 0.15 and *x* = 0.2, respectively, smaller than those of the single phase SSC cathode ($21.7 \times 10^{-6}\,K^{-1}$) and the dual-phase SSC–0.3BZCY cathode (*x* = 0) ($20.9 \times 10^{-6}\,K^{-1}$), which may be ascribed to the smaller TEC values of SDC ($12.8 \times 10^{-6}\,K^{-1}$) and BZCY ($11.2 \times 10^{-6}\,K^{-1}$) [10,13]. The average TEC values of triple-phase SSC–*x*SDC–(0.3 – *x*) BZCY (*x* = 0.1, 0.15, 0.2) composite cathode materials is closer to that of BZCY electrolyte than other cathode samples. This implies that the triple-phase composite materials might be more suitable for use as cathode for H-SOFCs based on BZCY electrolyte.

3.4. Electrical conductivity

Pure SSC materials possess mixed electronic and ionic (oxygen ion) conductivity at elevated temperatures owing to the co-presence of electronic holes and oxygen vacancies. However, the electronic conductivity is much larger than the ionic conductivity (by more than three orders of magnitude). Therefore, the values measured using the four-probe method can be treated solely as the electronic conductivity [14]. Similarly, SSC–*x*SDC–(0.3 – *x*) BZCY (*x* = 0, 0.1, 0.15, 0.2) composite cathode samples exhibit mainly the electronic conductivity because the ionic conductivity of SDC and BZCY electrolyte is so much small that can be ignored relative to the electronic conductivity. Fig. 4 shows electrical conductivity of the SSC and SSC–*x*SDC–(0.3 – *x*) BZCY (*x* = 0, 0.1, 0.15, 0.2) cathode specimens sintered at 1100 °C for 3 h. It is shown that electrical conductivity of all samples deceases gradually with increasing testing temperature, because as testing temperature increases, a substantial increase of thermally induced oxygen loss exists due to the electronic conductivity of these materials, decreasing not only the concentration but also the mobility of electronic carriers [13]. As shown in Table 2, the electrical conductivity of 354.8, 342.3, 303.1, 235.3 and 200.8 S cm^{-1} at 450 °C was acquired for the SSC, SSC–0.2SDC–0.1BZCY, SSC–0.15SDC–0.15BZCY, SSC–0.1SDC–0.2BZCY and SSC–0.3BZCY cathode samples, respectively. The SSC samples without any addition of electrolyte ingredients show the highest electrical conductivity among all the specimens. Because electrical conductivity

Table 2
Average thermal expansion coefficients (TECs) and electrical conductivity of the SSC and SSC–*x*SDC–(0.3 – *x*) BZCY cathode specimens sintered at 1100 °C for 3 h.

Cathode materials	Cathode material compositions			Electrical conductivity measured at 450 °C ($S\,cm^{-1}$)	Average TEC measured at 200–800 °C ($10^{-6}\,K^{-1}$)
	SSC (wt.%)	SDC (wt.%)	BZCY (wt.%)		
SSC	100	0	0	354.8	21.7
$x = 0$	70	0	30	200.8	20.9
$x = 0.1$	70	10	20	235.3	18.3
$x = 0.15$	70	15	15	303.1	18.0
$x = 0.2$	70	20	10	342.3	17.6

of the SSC–*x*SDC–(0.3 – *x*) BZCY ($x = 0, 0.1, 0.15, 0.2$) composite cathodes is affected by the added electrolyte materials, which only exhibits much low ionic conductivity without electronic conductivity. However, it is shown in Fig. 4 that electrical conductivity of the triple-phase SSC–*x*SDC–(0.3 – *x*) BZCY ($x = 0.1, 0.15, 0.2$) composite cathodes increases with the increase of SDC content. This may be ascribed to that the addition of SDC electrolyte can facilitate the sintering of composite cathodes and enhances the formation of a continuous lamellar microstructure (Fig. 2), which further improve the simultaneous transport of electronic defects for electronic conductivity. The electrical conductivity of the triple-phase composite cathodes is higher than 100 $S\,cm^{-1}$, which is adequate for the general requirement as cathode materials of SOFCs [15].

3.5. Electrochemical performance

Fig. 5 shows electrochemical impendence spectra of the symmetric cells with different cathode materials in air under open circuit conditions. An equivalent circuit of the cells is given in Fig. 6 for data analysis. Where L is the cable inductance, R_s is the overall ohmic resistance including the electrolyte, electrode, lead and contact between the cell and Ag mesh. R_1 and R_2 correspond to the electrode polarization resistances at low and high frequency, respectively. The sum of R_1 and R_2 corresponds to the total cathode polarization resistance (R_p). As shown in Fig. 5, each impedance spectra consists of two semicircles, indicating that there are at least two electrode processes for oxygen reduction reaction. The high-frequency arc is related to the polarization during the migration and diffusion of oxygen ions from the triple phase boundaries (TPBs) into electrolyte lattice, while the low-frequency one is due to the electrode polarization caused by the adsorption/desorption of molecular oxygen on the electrode surface [12,16]. It has been reported that SSC–BZCY cathode is very active for oxygen reduction because it allows the simultaneous transport of proton (H^+), oxygen vacancy ($V_O^{\bullet\bullet}$) and electronic defects (e' and/or $h^\bullet$), extending the active sites for oxygen reduction to a large extent and significantly reducing the cathode polarization resistance under fuel cell conductions [8]. However, AC impedance spectroscopy measurements of the symmetric cells in this work were conducted in air, and BZCY is a mixed proton and electron–hole conductor rather than a pure proton conductor under this condition. This weakens the difference in the polarization resistances between SSC–0.3BZCY composite and pure SSC cathodes, and the effects of adding BZCY on the polarization resistance of SSC are not very obvious (Fig. 5). Even so, the SSC–0.3BZCY cathode also exhibits less polarization resistance than pure SSC cathode at same test temperature (Table 3), which is consistent with the result that a proton conductor can be mixed with SSC to form a composite cathode to minimize the cathodic polarization resistance [17]. It can also be seen from Fig. 5 that polarization resistance of the triple-phase SSC–BZCY–SDC composite cathodes becomes even smaller than that of the SSC–0.3BZCY cathodes, and decreases evidently as SDC content increases. This could be attributed to that SDC shows high oxygen ion conductivity and enhances oxygen ion migration of triple-phase composite cathodes, since oxygen ion migration is a notable limiting step for cathodic processes of H-SOFCs [9].

The polarization resistances between BZCY electrolyte and different cathode materials determined from AC impendence spectra of the symmetric cells measured at various temperatures in air are presented in Fig. 7 and Table 3. It can be seen that the polarization resistance between each cathode material and BZCY electrolyte decreases significantly with the increase of measurement temperature, which implies that the ability of charge transfer on the electrode surfaces was significantly enhanced at high temperature. The value of polarization resistance is 8.15 $\Omega\,cm^2$, 2.80 $\Omega\,cm^2$, 1.55 $\Omega\,cm^2$, 0.99 $\Omega\,cm^2$ and 0.77 $\Omega\,cm^2$ for the SSC–0.2SDC–0.1BZCY cathode materials at 500 °C, 550 °C, 600 °C, 650 °C and 700 °C, respectively. However, the addition of SDC leads to dramatic increase in grain size and lower

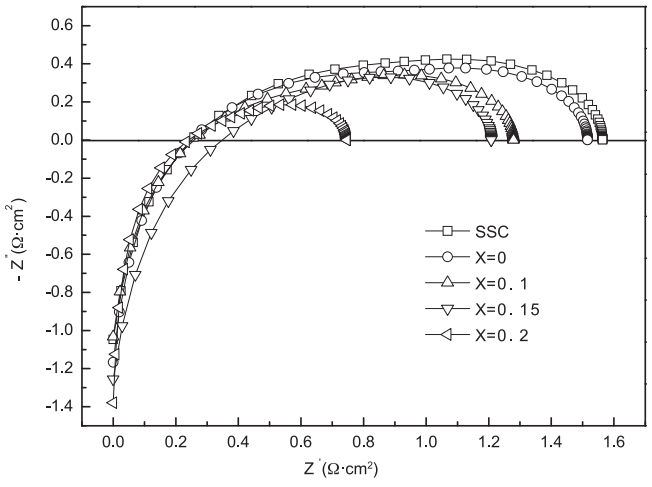

Fig. 5. AC impendence spectra of symmetric cells with different cathodes sintered at 1100 °C for 3 h measured at 700 °C in air under open circuit conditions.

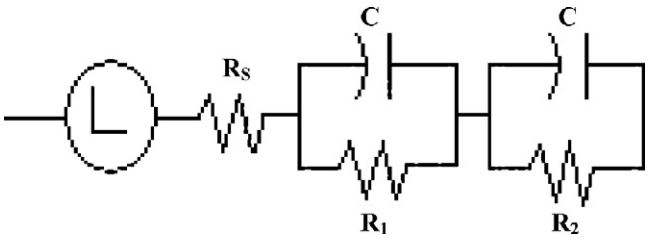

Fig. 6. The equivalent circuit used in analyzing the AC impedance spectra of the symmetric cells with different cathodes.

Table 3
Polarization resistances ($R_p/\Omega\,cm^2$) between the BZCY electrolyte and the SSC and SSC–xSDC–$(0.3-x)$ BZCY cathodes measured at different temperatures in air.

Cathode materials	Cathode material compositions			Testing temperature (°C)				
	SSC (wt.%)	SDC (wt.%)	BZCY (wt.%)	500	550	600	650	700
SSC	100	0	0	20.91	9.11	4.50	2.58	1.63
$x=0$	70	0	30	17.84	6.87	3.50	2.11	1.57
$x=0.1$	70	10	20	11.01	4.96	2.83	1.77	1.33
$x=0.15$	70	15	15	9.02	3.48	2.23	1.57	1.30
$x=0.2$	70	20	10	8.15	2.80	1.55	0.99	0.77

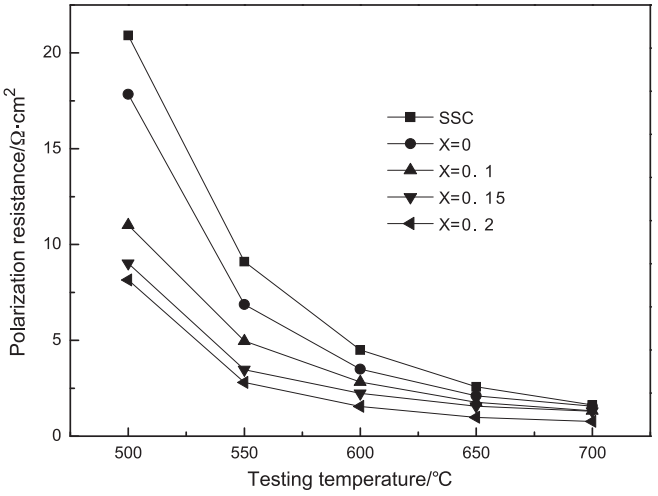

Fig. 7. Polarization resistances ($R_p/\Omega\,cm^2$) between BZCY electrolyte and different cathodes determined from AC impendence spectra of symmetric cells measured at different temperatures in air.

porosity in the triple-phase composite cathode materials, which might limit gas transportation to and from the reaction sites [18]. Consequently, additional improvement of electrochemical performance for the triple-phase composite cathode materials is possible by the optimization of their microstructure.

4. Conclusions

$Ce_{0.8}Sm_{0.2}O_{2-\delta}$ (SDC) and $BaZr_{0.1}Ce_{0.7}Y_{0.2}O_{3-\delta}$ (BZCY) electrolyte ingredients were added into $Sm_{0.5}Sr_{0.5}CoO_{3-\delta}$ (SSC) cathode to prepare triple-phase SSC–xSDC–$(0.3-x)$ BZCY ($x=0.1$, 0.15, 0.2) composite cathodes. SSC–0.1SDC–0.2BZCY composite cathodes sintered at 1100 °C for 3 h possess excellent chemical stability. The addition of SDC and BZCY into SSC cathode matrix can decrease the open porosity, increase the sintering shrinkage of SSC materials and significantly reduce the thermal expansion mismatch between BZCY electrolyte and SSC cathode. Electrical conductivity of the triple-phase SSC–xSDC–$(0.3-x)$ BZCY ($x=0.1$, 0.15, 0.2) composite materials can be enhanced by optimizing the amount of SDC electrolyte. The SSC–0.2SDC–0.1BZCY samples have an electrical conductivity ranging from 130.8 S cm^{-1} to 342.3 S cm^{-1} at temperature 450–800 °C. Polarization resistances between SSC–xSDC–$(0.3-x)$ BZCY ($x=0$, 0.1, 0.15, 0.2) composite cathodes and BZCY electrolyte decrease with the increasing SDC content. The value of polarization resistance is 8.15 $\Omega\,cm^2$, 2.80 $\Omega\,cm^2$, 1.55 $\Omega\,cm^2$, 0.99 $\Omega\,cm^2$ and 0.77 $\Omega\,cm^2$ for SSC–0.2SDC–0.1BZCY cathode sample at 500 °C, 550 °C, 600 °C, 650 °C and 700 °C, respectively. Based on present work, SSC–0.2SDC–0.1BZCY composition is suggested as suitable triple-phase composite cathode material for H-SOFCs, and further improvement of electrochemical performance of SSC–0.2SDC–0.1BZCY materials is possible by optimization of its microstructure.

Acknowledgements

This work is financially supported by the Natural Science Foundation of Anhui Province (contract no. 070414186), the Program of Science and Technology of Anhui Province (contract no. 2008AKKG0332), the Nippon Sheet Glass Foundation for Materials Science and Engineering (NSCF) (contract no. 070304B2) and the Open Project Program of Key Laboratory of Low Dimensional Materials & Application Technology (Xiangtan University), Ministry of Education of China (contract no. DWKF0802).

References

[1] R.T. Baker, R. Salar, A.R. Potter, I.S. Metcalfe, M. Sahibzada, J. Power Sources 191 (2009) 448–455.
[2] J. Dailly, S. Fourcade, A. Largeteau, F. Mauvy, J.C. Grenier, M. Marrony, Electrochim. Acta 55 (2010) 5847–5853.
[3] Y. Patcharavorachot, N.P. Brandon, W. Paengjuntuek, S. Assabumrungrat, A. Arpornwichanop, Solid State Ionics 181 (2010) 1568–1576.
[4] M. Asamoto, H. Yamaura, H. Yahiro, J. Power Sources 196 (2011) 1136–1140.
[5] E. Quarez, S. Noirault, A.L.G.L. Salle, P. Stevens, O. Joubert, J. Power Sources 195 (2010) 4923–4927.
[6] Y. Lin, R. Ran, Y. Zheng, Z. Shao, W. Jin, N. Xu, J. Ahn, J. Power Sources 180 (2008) 15–22.
[7] T. Wu, Y. Zhao, R. Peng, C. Xia, Electrochim. Acta 54 (2009) 4888–4892.
[8] L. Yang, C. Zuo, S. Wang, Z. Cheng, M. Liu, Adv. Mater. 20 (2008) 3280–3283.
[9] W. Sun, L. Yan, B. Lin, S. Zhang, W. Liu, J. Power Sources 195 (2010) 3155–3158.
[10] L. Yang, Z. Liu, S. Wang, Y. Choi, C. Zuo, M. Liu, J. Power Sources 195 (2010) 471–474.
[11] W. Sun, Z. Shi, S. Fang, L. Yan, Z. Zhu, W. Liu, Int. J. Hydrogen Energy 35 (2010) 7925–7929.
[12] B. Wei, Z. Lü, D. Jia, X. Huang, Y. Zhang, W. Su, Int. J. Hydrogen Energy 35 (2010) 3775–3782.
[13] Q. Xu, D. Huang, F. Zhang, W. Chen, M. Chen, H. Liu, J. Alloys Compd. 454 (2008) 460–465.
[14] Y. Guo, D. Chen, H. Shi, R. Ran, Z. Shao, Electrochim. Acta 56 (2011) 2870–2876.
[15] J. Xue, Y. Shen, T. He, Int. J. Hydrogen Energy 36 (2011) 6894–6898.
[16] X. Ding, C. Cui, L. Guo, J. Alloys Compd. 481 (2009) 845–850.
[17] T. Wu, R. Peng, C. Xia, Solid State Ionics 179 (2008) 1505–1508.
[18] C. Xia, W. Rauch, F. Chen, M. Liu, Solid State Ionics 149 (2002) 11–19.